Impact of Bioreactor Geometry on Mesenchymal Stem Cell Production in Stirred-Tank Bioreactors

Florian Petry and Denise Salzig*

Human mesenchymal stem cells (hMSCs) are manufactured as cell therapy products. This requires a tightly controlled and fully understood production process, usually taking place in a stirred-tank bioreactor. In this review, the impact of bioreactor geometry as well as equipment-related parameters is discussed. We provide a theoretical background for the engineering of hMSC spheroids with a defined size and evaluate the process parameters needed for the microcarrier-based expansion of hMSCs. Finally, and based on experimental data, ideal bioreactor setups for each type of process are recommended.

1 Introduction

The use of whole cells as active pharmaceutical ingredients is a new therapeutic paradigm. Thus far, 18 cell therapy (CT) products have been approved and hundreds of clinical trials are underway to test CT candidates targeting various diseases [1]. Among the key candidates for CT applications, human mesenchymal stem/stromal cells (hMSCs) are widely used due to their immunomodulatory and regenerative properties. Five hMSC products are already approved and 69 are in late-stage (phase 3) clinical trials (2021/04/15, clinicaltrials.gov, term: mesenchymal stem cells). Accordingly, there is a pressing need to develop large-scale, controlled and robust manufacturing methods for hMSCs.

The production of hMSCs involves several unit operations, including tissue sampling, cell isolation, cell expansion, cell harvesting, cell purification and CT product formulation, transport and storage. The cell expansion step is necessary to meet the dose requirements for CT because $100–150 \cdot 10^6$ cells are required per dose and such large numbers cannot be obtained directly by cell isolation [2].

Multiple cultivation systems are available for the expansion of hMSCs, including several types of flasks, G-Rex devices, fixed and fluidized bed reactors, hollow-fiber systems, wave bag reactors, vertical wheel reactors, the Zellwerk reactor, and rotating wall vessel reactors [3–10]. These systems can be classified as static or dynamic depending on the movement of the culture medium and cells. Static systems, where neither the medium nor the cells move, include classical tissue flasks and hyperflasks as well as the more recent G-Rex devices. In contrast, all reactor types are dynamic systems in which either the medium is moved while the cells remain in place (e.g., fixed-bed reactors, hollow-fiber systems, Zellwerk reactors) or both the medium

and the cells are moved (e.g., stirred-tank reactors (STRs), fluidized-bed reactors, wave bag reactors, and rotating wall vessel reactors).

There are three major cultivation strategies for hMSCs: (1) static monolayer cultures, (2) spheroids, and (3) adherent cell cultures in a bioreactor, typically in the form of microcarriers (MCs) in a STR (Fig. 1). Given that hMSCs are strictly anchorage dependent, the lack of a growth surface induces a form of programmed cell death known as anoikis. Static monolayer cultures are used for research and during early clinical development when small-scale production is sufficient. The growth surface is provided by plastic vessels such as T-flasks or multilayer stacked systems. These are easy to use and thus offer a reliable method to expand hMSCs. However, the flasks are open systems with limited monitoring and control. They rely on incubators to maintain the pH, CO_2 and O_2 levels, and process steps such as medium exchange and cell passaging are carried out manually, increasing the risk of contamination and process variation. A clean room environment is needed to maintain sterility, which increases the overall production costs. The available surface area is also restricted in monolayer systems, which limits scalability and introduces space constraints due to the low surface/volume (S/V) ratio. This is a particular drawback for allogenic hMSC products that

Florian Petry, Dr.-Ing. Denise Salzig
denise.salzig@lse.thm.de
University of Applied Sciences Mittelhessen, Institute of Bioprocess Engineering and Pharmaceutical Technology, Wiesenstraße 14, 35390 Giessen, Germany.
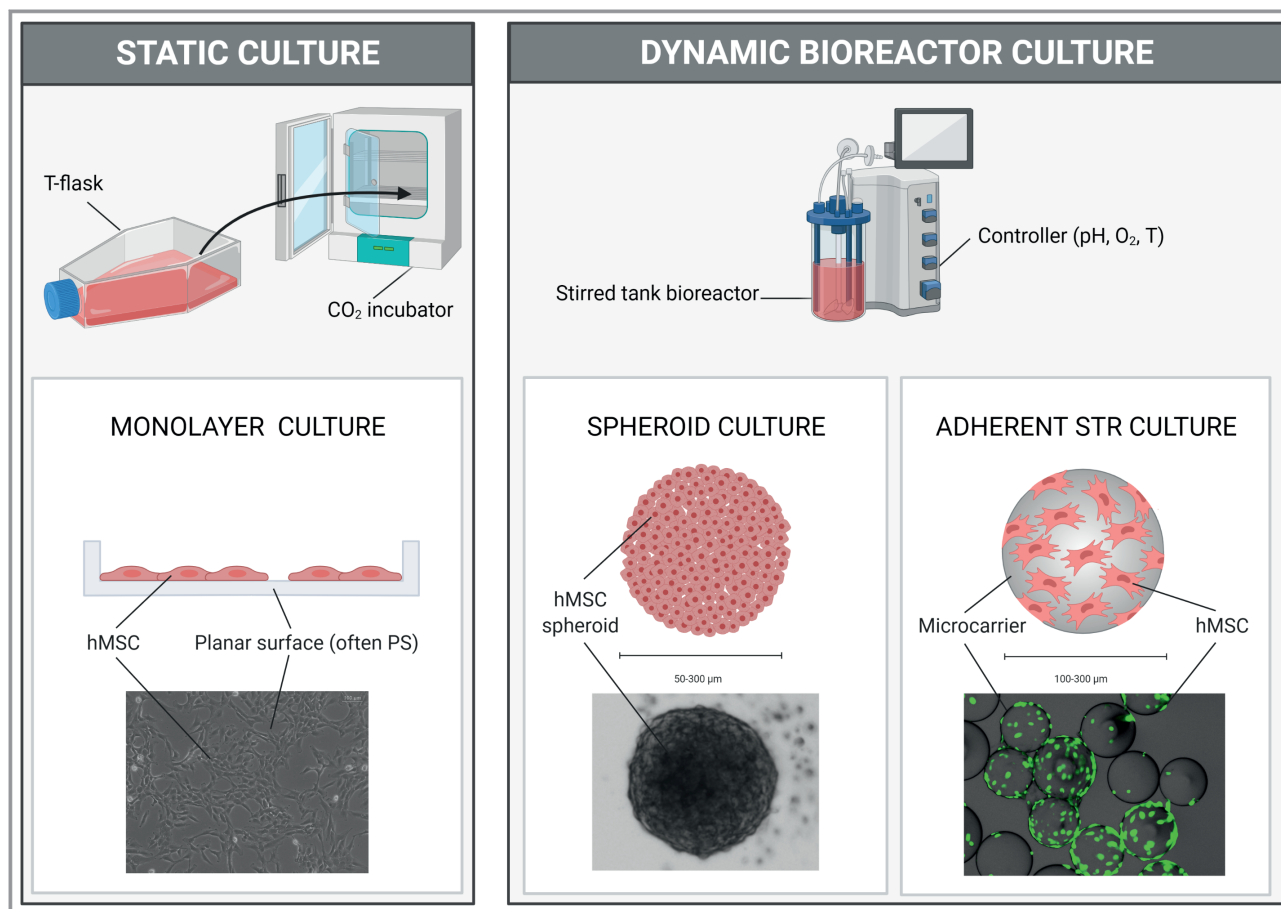
Figure 1. Overview of static and dynamic cultivation setups. Static cultures as monolayers in T-flasks are easy to handle but unsuitable for the large-scale 3D production of cell therapy products. Stirred-tank reactors overcome these limitations and facilitate the controlled and monitored production of stem cells as spheroids or on microcarriers. PS = polystyrene, T = temperature. This figure was created with BioRender (https://biorender.com/).

depend on economies of scale for cost-effective manufacturing, but also for autologous products where manufacturing is customized in scale-adapted processes.

The limitations of flasks can be overcome using bioreactor technologies, which improve scalability, enable process monitoring and control, and reduce dependency on human operators. The hMSCs can be cultivated in bioreactor systems as spheroids or adherent cells on carriers, fibers, or any other growth surface. For spheroid cultures, the main challenge is the control of spheroid size during cultivation. A large spheroid diameter causes the formation of a dead cell core and heterogeneous cell populations due to mass transfer limitations. The disaggregation of spheroids into single-cell suspensions is also challenging, but disaggregation is not always required because hMSC products can also be applied as spheroids. Several different concepts have been developed for the cultivation of adherent hMSCs in bioreactors, and in each case the key challenge is the provision of an ideal growth surface. This can be achieved by adding particles to the bioreactor – MCs in a stirred-tank bioreactor or macrocarriers in fixed-bed systems – or by integrating the growth surface into the bioreactor configuration (e.g., hollow-fiber reactors, the Zellwerk reactor, rotating bed/wall bioreactors, and vertical wheel bioreactors). In some bioreactor types (e.g., hollow-fiber and Zellwerk reactors), the aim is to cultivate three-dimensional hMSC aggregates. This is not the case for other bioreactor types, but such aggregates can be cultivated under certain process conditions. However, it is not clear whether this type of aggregation is beneficial, and in terms of harvesting efficiency and hMSC homogeneity such aggregates are disadvantageous.

The critical process parameters affecting hMSC growth must also be identified and controlled. These include classical parameters such as temperature, pH and dissolved oxygen (DO) but also more sophisticated and cell-specific parameters such as the hydrodynamic conditions, cell quality and in vitro cell age. Process development should also include a suitable process mode, agitation strategy, homogenization strategy, nutrient supply and medium. In this article, hMSC cultivation concepts in STRs are described and the challenges and bottlenecks as well as potential solu-

tions to facilitate the production of high-quality hMSCs are highlighted.

2 Requirements for Robust Production of hMSC-Related Products

CT products are defined as a specific class of advanced therapy medicinal product (ATMP) by the US Food and Drug Administration (FDA) whereas the European Medicines Agency (EMA) defines an equivalent category known as cell-based products. The production of hMSCs for CT applications falls under the guidance of the regulatory body overseeing the manufacturing process [11]. Furthermore, the specific application of each hMSC product determines the manufacturing process because different applications require different critical quality attributes (CQAs). The CQAs for hMSCs include the physical appearance of the formulation, cell number, viability, identity (e.g., cell phenotype or karyotype), purity (e.g., relating to process-related impurities, endotoxins, or microbes) and potency. The last of these in particular has an ambiguous meaning and directly links to the medical application and desired clinical outcome. A robust production process must ensure that the defined CQAs are achieved at all times.

Following cell isolation, the manufacturing process differs significantly for autologous and allogenic hMSC products and there are also major differences in the corresponding business models and supply chains. Allogenic hMSCs are intended for broad utilization and are sourced from one universal donor. The cells isolated from the donor are expanded for cell banking (master cell bank and working cell bank). From the working cell bank, the cells are expanded in large-scale bioreactors to create an off-the-shelf CT product. The design of manufacturing processes must guarantee the high quality and functionality of the cells and a sufficient number of cells for the intended application. In contrast, the production of autologous hMSCs involves the isolation of cells from the patient, followed by expansion and application to the same patient. This kind of personalized treatment requires small-scale bioreactors, and the bioreactor setup must therefore accommodate the properties of cells from different donors (e.g., differences in growth rate, attachment behavior, and shear resistance). An intelligent, automated and tightly controlled process is needed to minimize variation and guarantee process stability.

The expansion of hMSCs in a bioreactor is necessary to meet the defined CQAs, and most expansion studies are based on STRs because they are easy to use and scale up [11, 12]. STRs also achieve good aeration and mixing, and offer flexibility in terms of process setup, monitoring and control. Classical cylindrical STRs have a long history in the biopharmaceutical industry, and a large body of theoretical and experimental data dealing with transport phenomena (oxygen transfer, heat transfer, power consumption, and fluid dynamics) can be exploited during process develop-

ment [13, 14]. Traditional STRs are made of glass or stainless steel, but single-use systems are now available with scales ranging from 0.5 to 6000 L. STRs are mechanically driven, which means that the agitator/stirrer/impeller enables heat and mass transfer, aeration, and mixing for homogenization. Several other geometric specifications contribute to the performance of the STR, including the stirrer off-bottom clearance, the stirrer size, the baffles and their width, the aeration system, the ratio of liquid height to tank diameter, and the overall shape of the vessel (vessel height to diameter ratio) [15].

Given their fragility, hMSCs are highly sensitive to hydrodynamic forces [6] and bubble damage in the STR. The principal mechanisms that can lead to physical cell damage are hydrodynamic shear, tensile and compression forces induced by agitation [16], and air bubble damage caused by gas sparging. These aspects must therefore be considered carefully when designing processes for hMSCs.

3 Cultivation of hMSCs as Spheroids

Spheroids are attractive for CT because they mimic the native origin of hMSCs by providing a 3D microenvironment with a cell-specific extracellular matrix (ECM). This allows hMSCs to establish 3D networks without polarity, and spreading is sterically hindered. Such conditions facilitate cell-cell communication and overall tissue regulation similar to that taking place in vivo, thus improving cell viability and functionality (therapeutic effect). The hMSC spheroids adopt a more in vivo-like behavior than individual cells, with delayed replicative senescence and a more active secretome, as indicated by the 100-fold increase in the secretion of vascular endothelial growth factor (VEGF), the upregulation of stem cell marker genes, and higher survival rates after transplantation [17–20].

Most studies on the cultivation of spheroids involve static small-scale formats such as 96-well plates and common agglomeration techniques such as hanging drops, cell-repellent surfaces, self-assembly, or forced agglomeration [17]. These systems are sufficient for research but cannot satisfy the needs of CT manufacturing or drug testing studies. Spheroids with a defined size and high functionality are required for the controlled and monitored large-scale production of hMSCs. The bioengineering requirements for such processes are discussed below, and we consider different process setups for the large-scale production of spheroids.

3.1 Overview of Spheroid Cultures

The formation and maintenance of spheroids is challenging due to the presence of external forces. The ability of hMSCs to form spheroids can vary depending on the cell origin and cultivation setup (static vs dynamic) [21–23]. The concepts

of static (no fluid movement) and dynamic (cells are suspended and transported in moving fluid) spheroid formation are fundamentally distinct. Static spheroid formation techniques force the cells into a spheroid using hanging drops or cell-repellent well surfaces. These make the cells interact with each other due to the parabolic shape at the lowest point, where no other surface is available. Dynamic spheroid formation in a STR occurs when the suspended cells collide, which statistically gives a minimum cell concentration required to form spheroids. Furthermore, dynamic spheroid cultivation begins with an agglomeration phase, which lasts until a stable spheroid is formed, followed by a spheroid cultivation/growth phase. During the initial phase, the cell concentration is constant, and no cell division is thought to occur. This is analogous to the lag phase of standard monolayer cultures. Cell adhesion is dependent on the adhesion force F_{ad} and dissociation constant k_{cell} between two cells. The adhesion force and dissociation constant are cell-specific and strongly dependent on factors such as the ECM composition and culture conditions, so empirical testing is required. Initial agglomeration is dependent on homophilic cadherin/integrin interactions and ECM proteins [21]. The initial formation of a stable spheroid is followed by the buildup of an extended ECM, at which point hMSCs within the spheroid typically lose up to 75 % of their volume [18, 24–26]. The spheroids are continuously rearranged and condensed [18]. This is supported by experimental data that we and others have published [27] showing that spheroid size declines with cultivation time. Others have reported hMSC spheroid growth with cultivation time [28], but this also leads to an increasing number of single cells or smaller cell agglomerates in the supernatant, which can form new spheroids.

Importantly, the size of the resulting spheroids is a CQA. Spheroids are formed without vascularization, so mass transfer within the spheroids is limited to diffusive processes. This leads to the development of gradients with high concentrations of nutrients and oxygen on the outer layers and decreasing concentrations toward the spheroid core. In contrast, metabolic end products such as lactate accumulate in the spheroid core and decrease in concentration along the radial pathway [22, 29, 30]. Accordingly, the maximum size of viable spheroids is restricted by the consumption/production rates of the cells to prevent mass transfer limitations, which inhibit cell proliferation and trigger the formation of a necrotic spheroid core and ultimately a major loss of quality. The diffusive distance of oxygen in stem cell spheroids is 100–150 µm [30, 31], which limits the spheroid size to ~300 µm. Furthermore, the mass transfer gradients can induce the differentiation of hMSCs exposed to low or high concentrations of oxygen or nutrients, which can alter the metabolic state from the tricarboxylic acid cycle (normoxia) to anaerobic glycolysis (hypoxia) [30]. The regulation of spheroid size can also be used deliberately to induce differentiation along a certain pathway, but the homogeneity of differentiation within the spheroid is unclear. The

assessment of oxygen transfer within hMSC spheroids follows the Fick laws, as discussed elsewhere [32–35]. The minimum size of a spheroid also depends on the CT application. For example, many hMSC-based approaches involve the injection of single-cell suspensions or spheroids into the liver. In the case of single-cell suspensions, the fate of most of the cells is unknown, whereas the injection of spheroids results in a higher recovery rate. Spheroids of ~40 µm become trapped within liver vessels and realize their therapeutic effect. This imposes a functional size range of 40–300 µm for stem cell spheroids intended for CT. On this basis, the cultivation of spheroids differs from the cultivation of static monolayers or MCs, where mass transfer is not limited and the forces during expansion range from none (static) to highly variable (dynamic).

3.2 Impact of Reactor Geometry and Equipment-Related Parameters on Spheroid Size

The hydrodynamic forces applied during the expansion of hMSCs in bioreactors must be low because the fragile cells have no protective wall. The literature gives a broad range of critical shear forces for mammalian cells, from $1.2 \cdot 10^{-5}$ to $7.8 \, \text{N m}^{-2}$ [36, 37] and for hMSCs up to $2.5 \, \text{N m}^{-2}$ [9, 38]. The effect of shear stress depends on the cell type. For example, Chinese hamster ovary (CHO) cells can withstand up to $32 \, \text{N m}^{-2}$ [39]. It also depends on the measurement method (rheometer, flow chamber or STR), the flow regime (laminar vs turbulent), and the duration of the forces. The forces in laminar test systems must be greater than those in turbulent flow regimes to achieve the same damage [13, 40]. It is therefore important to understand and assess the cell stress in dynamic systems such as STRs during process design.

The cell stress in STRs involves a combination of (1) hydrodynamic stress reflecting the forces between the culture medium and the hMSCs due to different relative velocities, (2) the stress of cells colliding with other cells, the bioreactor wall, or the stirrer, and (3) gas-related stress, induced by gassing and the implosion of gas bubbles. The effect of collisions between cells and the stirrer, or cells and the bioreactor walls can be ignored in the case of hMSCs, given the minimal density differences and low cell/spheroid concentrations [13]. In small-scale bioreactors, and to simplify our model, we can also disregard the influence of gassing due to the low oxygen uptake rate of hMSCs ($90–300 \, \text{fmol cell}^{-1}\text{h}^{-1}$ [36, 41, 42]) and the corresponding low gas input. Scale-up requires further investigations of the influence of gas bubbles on spheroid formation. The hydrodynamic stress caused by different relative velocities is therefore the critical factor and can be divided into tensile, compression-induced and shear stress. In an STR, the power input by the stirrer is heterogeneous, which leads to pressure differences between different areas of the reactor. Areas with accelerated flow regimes are associated with

tensile stress on the cells/spheroids, whereas areas with de-accelerated flow lead to compression-induced stress [16]. The relative movement of fluid layers with different velocities results in shear stress on the cells. Depending on the stirrer setup and pumping (axial vs radial), the environment can be dominated by shear, tensile or compression-induced stress. Axial pumping stirrers might play a special role because these stirrers confer higher particle stress that cannot be explained by shear stress alone [16].

The most widely used model of hydrodynamic stress is Kolmogorov's theory of isotropic turbulence, which describes the energy input as a cascade of eddies decreasing in size and kinetic energy. Due to the viscosity of the fluid, the energy of the smallest existing eddies λ (Kolmogorov length) is converted to heat. The conversion of mechanical energy (from the stirrer) into heat is called energy dissipation. The application of Kolmogorov's theory gives a good correlation between the local energy dissipation and the local kinetic energy of the culture medium [43]. Therefore, our approach is to balance the local kinetic energy of the culture medium (and the resulting tensile/shear forces) with the strength of the spheroids, based on the adhesion force between individual cells [44–48]. Here, the stress acting on the spheroids depends on the inertial or dissipation range. Spheroids in the inertial range are more susceptible to breakage by tensile stress, whereas spheroids in the dissipation range experience stress as surface erosion (shear stress) [44–46]. To the best of our knowledge, the engineering of spheroids with a defined size has not been described in the literature, so we adapted concepts from empirical data representing model floc systems such as clay, latex, glass and other particles [33, 44–49].

3.3 Theoretical Estimation of Fluid Dynamics Affecting Spheroid Size

The flow patterns within STRs can be categorized as laminar, transitional or turbulent flow regimes. To predict such flow patterns, the Reynolds number Re is used to express the ratio of inertial forces to viscous forces in the culture medium:

$$Re = \frac{nd_S^2}{\nu_L} \tag{1}$$

where n is the stirrer frequency (also known as stirrer speed), d_S is the stirrer diameter, and ν_L is the kinematic viscosity of the culture medium. In the case of hMSC expansion, the effect of gas is ignored, and the flow pattern is mainly dependent on the power input P of the stirrer:

$$P = N_P \rho_L n^3 d_S^5 \tag{2}$$

where n and d_S are defined above, N_P is the dimensionless power number of the stirrer and ρ_L is the density of the liquid ($\sim 1004.3\,\text{kg}\,\text{m}^{-3}$ in the case of hMSC medium

supplemented with 10 % serum). The power number needs empirical validation and is proportional to the Reynolds number ($N_P \propto Re^{-1}$) within the laminar range ($Re < 20$), but it becomes constant and independent of Re in turbulent flow regimes due to isotropic fluctuation and loss of influence by the viscosity of the fluid. If we assume complete baffling is essential and therefore the absence of aeration (only headspace), fully developed turbulent flow occurs at $Re > 5000–10\,000$ and consequently N_P is constant [13]. Fully developed turbulent flow within the STR is necessary to achieve isotropic turbulence, which leads to a more homogenous distribution of the hydrodynamic forces and thus the stress on the spheroids compared to the changing behavior of the transitional range. In contrast, overall laminar flow does not provide the necessary shear forces for spheroid formation.

The hydrodynamic shear stress τ on hMSCs during laminar flow reflects the movement of liquid layers at different relative velocities. The scale of laminar shear stress can be described by the dynamic viscosity η and the shear rate $\dot{\gamma}$ [13]:

$$\tau_L = \eta \dot{\gamma} \tag{3}$$

During turbulent flow, the different relative velocities of the turbulent fluctuations confer kinetic energy on the cells, and the shear stress within turbulent flow regimes can be estimated based on the density ρ_L of the culture medium and the turbulent fluctuation velocity u [13]:

$$\tau_T = \rho_L \sqrt{u^2} \tag{4}$$

In Kolmogorov's theory of isotropic turbulence, the turbulence is characterized by a cascade of eddies declining in size and energy level. Therefore, u is connected to the eddy size and eddies similar in size to the spheroids are most relevant for balancing hydrodynamic forces against spheroid strength. This requires an estimation of the present eddy cascade and the allocation of spheroids to the corresponding Kolmogorov length. The eddy cascade can be divided into macroscale and microscale eddies. For Rushton turbines and pitched-blade Rushton turbines, the initial size of the macroscale eddies Λ_0 is proportional to the height of the stirrer h_S and can be described as [43]:

$$\Lambda_0 \approx \frac{h_S}{2} \tag{5}$$

The anisotropic macroscale eddies have the highest kinetic energy and are essentially influenced by the geometric arrangement of the bioreactor, such as baffling, the number and installation height of stirrers, or the stirrer type and the connected swept volume V_S (injection area) by the blades (blade angle, form and size). The evaluation and selection of stirrers is therefore important, depending on the intended function during cultivation (homogenization, suspension of particles or dispersion of gas). In contrast, the isotropic microscale eddies are not influenced by reactor

geometry (stirrer, baffling) and can be subdivided into inertial and dissipation ranges. As the term suggests, inertial forces dominate the inertial range, whereas the viscosity of the fluid is not relevant. In the dissipation range, the frictional resistance of the fluid becomes the prevalent phenomenon by the conversion of the kinetic energy of the (now laminar) flowing eddies into heat. According to Kolmogorov's theory, eddies in the dissipation range are only dependent on the kinematic viscosity ν_L and the specific energy dissipation ε (or $\bar{\varepsilon}$, mean dissipation rate per mass unit m). The smallest existing eddies λ can be calculated as follows:

$$\lambda = \left(\frac{\nu_L^3}{\varepsilon} \right)^{0.25} \tag{6}$$

where

$$\varepsilon \propto \bar{\varepsilon} = \frac{P}{m} = \frac{N_P n^3 d_S^5}{V_L} \tag{7}$$

All stirrers have a specific power number N_P (or P_0) reflecting the moment of resistance. N_P reaches a constant value under fully developed turbulence and needs empirical verification or can be adopted from comparable systems or Newton-Reynolds diagrams. The determination of N_P is mainly based on torque measurement, which can be affected by the bearing of the stirrer shaft. The adaption of N_P is only valid when the geometric setup is similar, such as d_S/D_T, stirrer height from the bottom, or H_L/D_T.

The energy dissipation within STRs is heterogeneous and strongly influenced by the stirrer type. The maximum energy dissipation ε_{max} is found immediately adjacent to the stirrer ($= V_S$) and is more than 10 times higher ($\varepsilon_{max} < 10\bar{\varepsilon}$) than at more distant locations [43]. With full turbulent flow in a defined geometric setup, the maximum energy dissipation ε_{max} is constant and the $\varepsilon_{max}/\bar{\varepsilon}$ ratio can be used as a criterion specific to the reactor. The local energy dissipation is usually unknown, and the cells/spheroids circulate with a certain frequency and residence time through the high-shear-stress zones close to the stirrer, known as the energy dissipation circulation function (EDCF). Accordingly, we aim to minimize $\varepsilon_{max}/\bar{\varepsilon}$ as much as possible when setting up the STR. The EDCF describes the energy dissipated by the specific stirrer swept volume V_S combined with the circulation time t_C. The EDCF concept is mainly used for the destruction or modulation of mycelial morphology by shear stress and can be applied to multiple stirrer types and scale-up criteria [50, 51]. The precise energy dissipation lies somewhere between the lowest energy dissipation ε_{low} and ε_{max}, but a narrow spheroid size distribution is associated with the homogenous distribution of the power input within the STR.

Based on the points discussed above, the adjustment point $\bar{\varepsilon}$ to engineer spheroids of a given size depends on the stirrer, the specific power input, and the reactor geometry. The kinetic energy (turbulent fluctuation velocity u) at a distance Δr between two adjacent points in the velocity field is dependent on the eddy size [13]. As stated above, the size and distance of eddies (fluid layers) similar in size to the spheroids ($\Delta r = d_{Sph}$) are relevant to our assessment and engineering of spheroids with a defined size. In relation to the smallest existing eddies λ, the range in which the spheroid size of interest is affected can be estimated as follows [13, 43]:

Inertial range:

$$25\lambda < d_{Shp} < 0.1\Lambda_0 \tag{8}$$

Dissipation range:

$$d_{Shp} < 6\Lambda_0 \tag{9}$$

Eqs. (8) and (9) are only valid under turbulent conditions, which requires that macroscale turbulence is independent from the viscosity [13]. The separation of the macroscale and dissipation range is based on the ratio Λ_0/λ, which expresses current energy levels. Eq. (10) is used to calculate a sufficient separation of the macroscale and dissipation range [52]:

$$\frac{\Lambda_0}{\lambda} = \left(\frac{\Lambda_0 \bar{\varepsilon}^{0.25}}{\nu_L^{0.75}} \right) > 125 \ldots 250 \tag{10}$$

The development of an inertial range can be particularly difficult in small bioreactors, and Λ_0/λ is relevant to ensure a turbulent pattern.

Importantly, the hydrodynamic stress on the spheroids depends on d_{Sph}/λ. Ratios of $d_{Sph}/\lambda > 3$ lead to tensile stress acting on the spheroids [44]. Higher tensile forces in the culture medium cause the spheroids to break into smaller fragments. A steady-state spheroid size is achieved by balancing the hydrodynamic tensile forces σ_T against the adhesion force of adjacent single cells within the spheroid. These hydrodynamic tensile forces can be estimated as follows [44, 46]:

$$\sigma_T = (1 - P_F) \frac{F_{ad}}{d_{cell}^2} \tag{11}$$

where P_F is the spheroid porosity:

$$(1 - P_F) = \left(\frac{d_{cell}}{d_{Sph}} \right)^k \tag{12}$$

For monodisperse glass spheres agglomerated with polyacrylamides, $k = 1$ [44]. For hMSCs, k needs empirical verification and is dependent on the nature of the adhesion forces between single cells. Goodman et al. [53] determined porosities for tumor spheroids in a range from 0.01–0.5, from which we can approximate values of k between 0.003–0.22.

The size-limiting process for $d_{Sph}/\lambda < 3$ can be reduced to surface erosion due to shear forces affecting the outer surface of the spheroid. A pseudo-surface tension δ_{Sph} can

be introduced to estimate the hydrodynamic shear force σ_S [44]:

$$\sigma_S = \frac{\delta_{Sph}}{d_{Sph}} \tag{13}$$

where the pseudo-surface tension δ_{Sph} is defined as:

$$\delta_{Sph} = (1 - P_F) \frac{F_{ad}}{d_{cell}} \tag{14}$$

Considering the required power input ($\sim 0.01\,\mathrm{W\,kg^{-1}}$) to achieve fully developed turbulent flow, the surface erosion is expected to be more relevant than the tensile stress, and we therefore focus on the formation of spheroids guided by shear stress. The fluctuation velocities for the dissipation range, which is needed to determine the turbulent shear stress from Eq. (4), can be assessed as follows [13]:

$$\sqrt{\overline{u^2}} = 0.0676 d_{Sph}^2 \frac{\bar{\varepsilon}}{\nu_L} \tag{15}$$

We now consider the path of cells through the turbulence cascade after inoculation. On the macroscale, the cells are transported convectively along the streamlines of eddies decreasing in size until the cells reach the laminar flow of the dissipation range. Here, the cells collide, bond, and form small agglomerates. These small agglomerates grow larger (by attachment to other cell aggregates or the further attachment of individual cells) until the shear forces of a certain eddy size are too high and further cell connections are prevented. The balance between the potential surface energy of a spheroid (bonding energy E_{Bond}) and the kinetic energy E_{Kin} at a certain eddy size (similar to spheroid size) is therefore crucial to produce spheroids with a defined size.

$$\frac{E_{Kin}}{E_{Bond}} = 1 \tag{16}$$

Using the fluctuation velocity from Eq. (15), the kinetic energy of the surrounding fluid within the dissipation range can be described as follows:

$$E_{Kin} = \frac{\pi}{4} \rho_L \sqrt{\overline{u^2}} d_{Sph}^3 = \frac{\pi}{4} \tau_T d_{Sph}^3 \tag{17}$$

The bonding energy E_{Bond} can be derived from Eq. (13) and the surface of the spheroid:

$$E_{Bond} = \delta_{Sph} \pi d_{Sph}^2 = (1 - P_F) \frac{F_{ad}}{d_{cell}} \pi d_{Sph}^2 \tag{18}$$

The adhesion force F_{Ad} and shear stress can be used to estimate the size of the resulting spheroids as follows:

$$d_{Sph} = \frac{4\delta_{Sph}}{\tau_T} \tag{19}$$

Eq. (19) clearly shows that increasing the power input and related energy dissipation increases the shear stress and

thus reduces the size of cell aggregates. Furthermore, the size of the crucial eddies must be similar to the desired spheroid size. Eddies much larger in size than the critical spheroid size transport the spheroids convectively along the streamlines [43]. Although the determination of F_{Ad} and thereby the pseudo-surface tension is challenging and requires further research, the floc or agglomerate/spheroid strength can be determined empirically.

The strength of agglomerates and the path to agglomeration or splitting at different power inputs has been discussed in detail [47, 48]. Floc strength can be measured using a cantilever [54]. The following empirical approach can also be used to determine the agglomerate strength [55]:

$$d_{Sph} = C_{Agg} \varepsilon^{-n} \tag{20}$$

where C_{Agg} is the aggregate strength coefficient (we use the index "aggregate" rather than spheroid because the concepts have been adopted from particle process engineering) and exponent n ranges in value from 0.25 to 0.47. Both C_{Agg} and n need empirical verification and we determined a spheroid strength of $325\,\mathrm{N\,m^2}$ for a model cell line. The spheroid strength is based on the adhesion force F_{ad} between the cells and is established by different membrane proteins. F_{ad} therefore depends on multiple factors, such as the cell type, the culture medium, and the harvesting method. For example, hMSC expansion media often contain fetal calf serum featuring hundreds of mostly unknown proteins. Some serum proteins interfere with the agglomeration process by a masking the cell surface proteins, whereas others (such as laminin or fibronectin) promote cell-cell interactions. Cell adhesion is mediated by surface proteins that interact with receptors on adjacent cells, in the ECM, or on surfaces [21]. F_{ad} is therefore directly proportional to the number of these specific surface proteins, including cadherins responsible for cell-cell interactions and integrins responsible for the binding of cells to other cells and the ECM [21, 56]. For context, a single fibroblast can display $\sim 2 \cdot 10^5$ integrins on its surface and if only 10 % of them are engaged it would take $400\,\mathrm{N\,m^{-2}}$ of force to detach the cell [56]. Because these adhesion proteins are located on the cell surface, enzymatic harvesting methods using trypsin can modify the agglomeration behavior of the cells due to the loss of the adhesion proteins. The adhesion force should be measured using a method that takes in account factors such as the medium and enzymes, enabling transfer to the STR. Most importantly, the shear stress should represent a turbulent regime. Brief exposure to turbulent velocities causes the abrupt detachment of cells from their growth surface, whereas the same velocities in a laminar regime lead to stepwise detachment of the surface proteins, and thus take longer [56]. This demonstrates the complexity of interactions between cells and other cells, the ECM and surfaces.

3.4 Recommended STR Setup to Generate Spheroids of Defined Size

The design of the bioreactor facilitates the shear-guided formation of spheroids. However, this does not mean that the shear stress can be increased to reach the desired spheroid size. Instead, the shear stress must be balanced within a narrow working range that minimizes cell damage but allows aggregation. This can be achieved by knowing the maximum force tolerated by the cells and sufficient to ensure homogenous distribution of the energy dissipation in the bioreactor. The energy distribution is primarily influenced by the stirrer, the baffles, and the reactor geometry.

The function of the stirrer is to suspend the cells/spheroids homogenously within the STR, create a turbulent flow, and ensure proper mixing and sufficient mass transfer. There are many stirrer options that maximize energy transfer while balancing the shear forces in the system. Stirrers can be categorized according to their fluid pumping characteristics. In our system (low viscosity, water-like liquid) appropriate stirrers fall into two broad categories: axial and radial flow. However, the multiple functional demands on the stirrer have led to the development of many variants and subtypes with combined characteristics, including radial and axial pumping stirrers, three-segment pitched-blade (3-SPB) stirrers similar to an elephant-ear impeller, and innovative geometries such as cell-lift stirrers. The installation of multiple stirrers may be useful in some cases. The power number N_P is often associated with the particle stress of the stirrer (high N_P values equate to high particle stress) and is a good indicator of the power characteristics (particle stress), but it ignores the reactor geometry.

Axial pumping stirrers such as the marine propeller/impeller drive bottom-to-top fluid movement and are mainly used for suspension. Henzler et al. [13] and others [14, 16, 50, 51] reported that axial flow stirrers with lower N_P values than radial flow stirrers such as the Rushton turbine (N_P ~4–5) cause higher particle stress at the same specific power input. In such cases, particle stress might be explained by higher particle frequencies and residence times in the swept volume of the stirrer (V_S). The destructive effect within V_S (ε_{max}) is caused by the trailing vortices of the stirrer blades. Here, axial and radial stirrers differ in the structure and number of the vortices, with axial stirrers inducing higher tensile and/or compression-induced stress. A correction factor k' for the EDCF has been introduced to accommodate differences in the trailing vortices of each stirrer type [50].

Particles or cells exposed to tensile stress do not rotate and thus experience selectively higher particle deformation compared to rotating cells within shear stress areas, leading to the homogenous distribution of forces on the cell/spheroid surface [16]. This gives axial pumping stirrers a special role and might explain the use of 3-SPBs for cell culture processes, combining the characteristics of axial and radial stirrers.

Rushton stirrers are mostly used for microbial cultures but can be useful for mammalian cell cultures too. When combined with an axial flow stirrer, a Rushton stirrer improves mixing, reduces power requirements, and alters shear force characteristics [57]. The selection of an appropriate stirrer is essential for the gentle formation of spheroids with a defined size. The shape and pumping direction are key parameters, but the interplay with the bioreactor setup must also be considered, such as the d_S/D_T and h_S/d_S ratios and the use of sufficient baffles. Lower d_S/D_T and h_S/d_S ratios reduce the stirrer swept volume to reactor volume ratio (V_S/V_L) and decrease the particle diameter in a reference floc particle model. In the case of the disc stirrer, the low h_S/d_S ratio (~0) can cause high shear forces that destroy agglomerates [13, 14]. This phenomenon is based on the large differential between the relative velocity of the rotating disc and the surrounding fluid combined with the missing blades/areas (injection areas) to reinforce the power input to the fluid. In the context of energy dissipation, ε_{loc} in proximity to the disc is extremely high. Weakened effects of this behavior can be assumed for axial flow stirrers depending on the angle of the blades (smaller angles induce more shear stress). Interestingly, the shear stress is not only increased by small blade angles but also by reducing the number of blades, meaning that a smaller injection area to reinforce the power input leads to higher particle stress [13]. In our case, the selection of an appropriate stirrer is based on minimizing the $\varepsilon_{max}/\bar{\varepsilon}$ ratio by utilizing stirrers with reduced high local energy dissipations in close proximity to the blades (depending on stirrer design) and increasing the stirrer swept volume V_S. Many strategies have been proposed to estimate $\varepsilon_{max}/\bar{\varepsilon}$, which are mainly based on Rushton turbines [40, 52, 58, 59]. Wollny et al. [43] and Henzler et al. [13] use similar correlations to estimate this ratio, including geometric properties such as d_S/D_T, h_S/d_S and H_L/D_T, the angle of the stirrer blades ($\sin\alpha$), the number of blades z_B, and the number of installed stirrers z_S.

$$\frac{\varepsilon_{max}}{\bar{\varepsilon}} = 0.84 N_P^{1/3} \left(\frac{D_T}{d_S}\right)^3 \left(\frac{H_L}{D_T}\right) \tag{21}$$

$$\frac{\varepsilon_{max}}{\bar{\varepsilon}} = \frac{4}{\left(\frac{d_S}{D_T}\right)^2 \left(\frac{h_S}{d_S}\right)^{2/3} z_B^{0.6} \sin\alpha^{1.15} z_S^{2/3} \left(\frac{H_L}{D_T}\right)^{-2/3}} \tag{22}$$

Eq. (21) from Wollny et al. [43] is mostly dependent on the power number N_P, which includes information about the stirrer design and arrangement in the STR. However, without installed baffles and/or a non-established turbulent flow, especially for small bioreactors, N_P is not constant and leads to a poor assessment of $\varepsilon_{max}/\bar{\varepsilon}$. Eq. (22) from Henzler et al. [13] instead uses a more stirrer-specific geometric function (V_S) and may better reflect real situations: a high $\varepsilon_{max}/\bar{\varepsilon}$ ratio for a radial stirrer (Rushton turbine, $d_S/D_T = 0.33$ and $h_S/d_S = 0.2$) and an increase in $\varepsilon_{max}/\bar{\varepsilon}$ for lower blade angles and fewer blades in the case

of an axial stirrer [13]. Eq. (22) provides valid data for $0.225 < d_S/D_T < 0.75$, $0.1 < h_S/d_S < 1$, $2 < z_B < 12$, $24° < \alpha < 90°$, $z_S = 1$ or 2, and $1 < H_L/D_T \leq 2$ [13]. Although Eqs. (21) and (22) are both derived from empirical data for the Rushton turbine, its application to other stirrer types gives a first insight in the distribution of the energy dissipation.

By achieving homogenous energy dissipation in the bioreactor, an ideal stirrer would apply stress (injection area) to the whole bioreactor volume ($V_S/V_L = 1$). Logically, $V_S/V_L = 1$ is not applicable and therefore the stirrer diameter d_S and height h_S should be maximized with respect to the corresponding stirrer pumping profile.

For axial pumping stirrers, such as pitched blade/marine impellers and 3-SPB devices, which rely on the redirection of flow from the bottom and thus cause friction, the stirrer installation height $h_{S,B}$ (from the bottom) or bottom clearance $C = h_{S,B}/d_S$ is relevant for appropriate reinforcement and design, thus influencing the power number [60, 61]. Heyter et al. [60] changed the bottom clearance from 0.2 to 0.56 and reported a small decrease in N_P (~7 %). In multi-stage systems, where bottom clearance resembles the distances between stirrers, the influence on the power number increases to 33 % [60].

As basic equipment for cell culture in an STR, we recommend a complete baffled vessel to achieve proper mixing, preventing the segregation of multiphase systems (Sect. 4) due to the influence of different densities and centrifugal forces [60, 62]. Specifications are often restricted to simple descriptions such as "non-baffled" or "complete baffling", and the latter means four baffles with a tank diameter to baffle width ratio of $D_T/B_W = 10–12$ and a $D_T/50$ clearance from the wall [60, 63]. Baffles reduce the velocity of tangential flow and redirect the flow into radial and axial regimes, resulting in turbulence [60]. This restricts the development of a vortex along the stirrer shaft and the rotation of the continuous phase along the stirring direction [63]. Furthermore, the installation of baffles enables a more homogenous distribution of the power input by the stirrer and reduces differences in local energy dissipation (small $\varepsilon_{max}/\bar{\varepsilon}$ ratios), thus achieving more homogenous particle (spheroid) stress [60]. The degree (index) of baffling/reinforcement B_I can be calculated as follows [61]:

$$B_I = c_F N_B^{0.8} \left(\frac{W_B}{D_T}\right)\left(\frac{H_B}{D_T}\right) \tag{23}$$

where c_F is a correction factor for non-planar baffles such as cylindrical probes ($c_F = 0.45$), N_B is the number of baffles, W_B the baffle width, and H_B the actual height of the baffle in the liquid phase. The relevance of reinforcement becomes clear when looking at the power number, which is strongly influenced by the bioreactor setup (stirrer geometry, d_S/D_T ratio, and degree of baffling). Heyter et al. [60] showed that, under turbulent conditions and increasing reinforcement, an increase in the power number occurred until a constant value was achieved by so-called complete baffling.

Complete baffling $B_{I,com}$ can defined by the following correlation [60]:

$$B_{I,com} \approx 0.36 \frac{d_S}{D_T} N_{P,com}^{0.33} \tag{24}$$

Heyter et al. [60] reported an increase in the power number from 4.3 ($B_I = 0.19$) to 4.7 ($B_I = 0.28$) for a Rushton turbine ($d_S/D_T = 0.36$, $H_L/D_T = 1$, and bottom clearance $C = h_{S,B}/d_S = 0.2$) and the same effect applied for a $4\times45°$-blade pitched turbine ($d_S/D_T = 0.6$, $H_L/D_T = 1$, and $C = h_{S,B}/d_S = 0.2$) with $N_P = 1.4$ at $B_I = 0.24$.

This means that small-scale systems such as spinner flasks without baffles are unsuitable for the assessment of hydrodynamic forces. The culture medium in the spinner flasks rotates in a laminar or transitional flow regime, and the results therefore do not represent a scaled-up process. In small-scale bioreactor processes (0.5–3 L) the installed probes for pH, DO or impedance act as additional baffles and improve the power input, mixing and homogenization. The development of turbulent flow requires sufficient discrimination between the inertial and dissipation range within the turbulence spectrum. Based on Eq. (10), the minimal reactor size can be estimated as follows [52]:

$$D_T > \frac{200}{\frac{\Lambda_0}{D_T}} \left(\frac{\frac{v_L^3}{\bar{\varepsilon}}}{\frac{\varepsilon_{max}}{\bar{\varepsilon}}}\right)^{0.25} \tag{25}$$

In conclusion, complete baffling ($B_{I,com} \geq 0.2$) is necessary to achieve the necessary turbulent flow regime ($Re = 5000–10\,000$) and maximum power input by the stirrer [13, 64]. The selection of an appropriate stirrer is therefore the main recommendation to achieve the shear stress-guided formation of spheroids. Entirely axial pumping stirrers are not recommended due to their reduced power reinforcement and resulting high particle stress. Combined (axial and radial) pumping with a 3-SPB stirrer may be the best option because these stirrers achieve a high V_S/V_L ratio ($\approx 0.12–0.2$) and a low $\varepsilon_{max}/\bar{\varepsilon}$ ratio (< 20). Eqs. (21) and (22) were applied to determine $\varepsilon_{max}/\bar{\varepsilon}$ under turbulent conditions and the same specific P/V for different stirrer types. The approach by Wollny [43] resulted in $\varepsilon_{max}/\bar{\varepsilon} = 5$ for a $30°$-3-SPB ($d_S = 0.065$ m) and $\varepsilon_{max}/\bar{\varepsilon} = 13$ for a Rushton turbine ($d_S = 0.054$ m). With both stirrer types, we were able to form spheroids of the estimated size (size calculated = 40 µm, measured size for both stirrer types = 40 µm). This indicated that the theoretical concepts presented here could be verified experimentally. Although Rushton turbines are associated with high local energy dissipation close to the stirrer tip, their radial pumping characteristics may be superior to axial stirrers [13]. Depending on the STR geometry and shape (U-bottom vs flat bottom), a Rushton turbine with a $d_S/D_T \geq 0.6$ may be appropriate to increase the V_S/V_L ratio. These stirrers are typically standardized ($d_S/D_T = 0.2–0.5$, $h_S/d_S = 0.2$, $z = 6$) so it may be difficult to

increase the h_S/d_S ratio. Even so, the selected stirrer should have a d_S/D_T ratio $\geq$ 0.4, a high h_S/d_S ratio, thus a high V_S/V_L ratio, and a bottom clearance of $C \approx 0.2$ [14].

4 Expansion of hMSCs Using Microcarriers

Most hMSC expansion studies in STRs are based on MCs rather than spheroids. In this section, we consider the unique aspects of process design for MC-based cell expansion in STRs ranging in scale from 100 mL to 50 L. Similar final cell densities of $2–4 \cdot 10^5$ cells mL^{-1} are usually achieved regardless of the scale or the source of hMSCs [65]. Several STRs with different geometries and stirrer configurations are already available, but systematic comparisons of their use for hMSC expansion have not been published.

4.1 Overview of Microcarrier Cultures

MCs are essential for the large-scale cultivation of adherent hMSCs because they overcome the limitations of traditional cultivation vessels [66]. Several MC types have been used for the expansion of hMSCs [67] but most are non-porous beads with a polystyrene core and different coatings or surface treatments (Tab. 1). The interaction between hMSCs and MCs is responsible for cell attachment, proliferation/ growth and detachment, but hMSCs from different sources (e.g., bone marrow, adipose tissue or umbilical cord) and

even hMSCs from the same tissue but different donors, have different requirements in terms of attachment [68]. This explains the broad range of MC types, and selection requires preliminary knowledge or empirical attachment experiments. Such experiments can be performed in small-scale systems such as spinner flasks, but once an appropriate MC has been selected the challenges of process development differ considerably from those pertinent to spheroid cultures. First, the STR must guarantee the homogenous suspension of the MCs and cells. Second, the suspended cells must attach to the suspended MCs, so the cell-specific adhesion force F_{ad} also plays an important role to enable the efficient attachment of hMSCs to the MC surface rather than to each other. Third, the cells must be distributed homogenously on the MCs to exploit the complete growth surface, which logically defines a minimum seeding density. Finally, a brief and gentle cell harvest is required, so the cell attachment strength must be balanced to enable cell detachment. The ideal MC would feature an adjustable F_{ad} depending on the process phase (high during attachment, low during detachment), which would require structural modification of the MCs or the addition of modifying factors during the expansion process. Various concepts have been explored for harvesting, including enzymatic cell detachment and MC disintegration. Importantly, MCs strongly affect the oxygen transfer rate, mixing properties and distribution of shear forces, which must be considered when setting up MC-based hMSC expansion processes.

Table 1. Overview of commercially available animal-free microcarriers suitable for hMSC expansion processes based on information from manufacturers' websites and documents. PS = polystyrene.

Manufacturer	Microcarrier	Core material	Coating (surface charge)	Size range [μm]	Growth area [cm²g⁻¹]	Density [g cm⁻³]	Working range [g L⁻¹]	Harvest method
PALL Corporation	SoloHill®, Hillex®	PS	Cationic amine-modified PS (+)	160–200	515	1.090–1.150	1–25	Enzymatic cell detachment
	SoloHill®, Plastic		Cross-linked PS (+/−)	90–150, 125–212	480, 360	1.022–1.030, 1.034–1.046		
	SoloHill®, Plastic Plus		Cross-linked PS (+)	125–212	360	1.022–1.030		
GE Healthcare	Cytodex1	Dextran	*N,N*-diethylami-noethyl (DEAE)-groups (+)	147–248	4400 (dry weight)	1.030	1–3	Enzymatic cell detachment or MC disintegration
Corning®	CellBIND®	PS	Facilitates oxygen transport, and hydrophilic (−)	125–212	360	1.026	1–25	Enzymatic cell detachment
	Synthemax II		Recombinant peptide-polymer					
	Enhanced Attachment		Facilitates oxygen transport, and hydrophilic (−)					

4.2 Impact of Reactor Geometry and Equipment-Related Parameters on hMSC Yield

When hMSCs are cultivated on MCs, shear stress and other forces should be minimized to avoid cell damage and loss of functionality, but the power input of the stirrer must be sufficient to maintain a homogenous MC and cell suspension. This establishes a working range for the stirrer and other equipment-related parameters.

Typical MCs are spherical particles similar in size to hMSC spheroids (100–300 µm in diameter) and they are subject to the same forces: (1) hydrodynamic stress on cells attached to MCs, (b) collision stress caused when hMSCs collide with MCs, the stirrer and the bioreactor walls, and (c) cellular stress induced by collisions between cell-laden MCs in suspension [69]. The equations from Sect. 3.2 can be used to assess the hydrodynamic stress and establish a set point for the upper power input range. Acceptable levels of shear stress that can be tolerated by adherent growing cells such as Vero cells vary from 3.5 to 5 N m^{-2} [70–72]. However, shear stress analysis is more complex for hMSCs. Depending on the required outcome (differentiation or the maintenance of multipotency), the culture system (bioreactor type), measurement method, and type of shear stress (laminar vs. turbulent), the literature provides values ranging from 0.0016 to 2.5 m^2 [9, 38, 73]. Eddies of the size $\lambda \geq \sim 0.6 d_{MC}$ do not damage hMSCs growing on MCs [74]. However, hMSCs adhering to MCs can experience more damaging forces due to the lower elasticity, higher stiffness and slightly higher density of the polystyrene-core MCs compared to compressible tissues and cells (80–90 % water, thus approximately the density of water). The adherent cells also have a lower degree of freedom than suspended cells/spheroids because the forces cannot be transferred into rotational or tensile movement, or cell compression [70, 75, 76]. MCs are also exposed to dragging forces caused by the motion of the medium, gravity and buoyancy, local pressure gradients, inertial and Magnus effects resulting from MC rotation, and viscous shear stress [69]. Kolmogorov's theory explains the stress acting on cells and MCs caused by eddies similar in size to the cells/MCs but eddies similar in size to the intermediate bead distance also cause damage by increasing the MC collision rate [69]. The shear forces caused by eddies in the MC size range can be estimated by setting the smallest eddy size λ as the mean MC diameter (150 µm). The resulting velocity of 0.5 cm s^{-1} causes the MCs to rotate at ~10 rpm, which exposes the cells on the surface to varying shear stress at 10 Hz [69]. Given the isotropic nature of the turbulent regime, the stress can be increased or decreased by multiple eddies acting simultaneously on the same MC [69]. MC collisions might be as relevant as hydrodynamic stress for the vitality and functionality of hMSCs. This is related to the MC concentration because MCs can be treated as liquid packages, and the collision rate depends on interactions between these packages. The frequency of such collisions can be assessed

using the so-called turbulent collision severity (*TCS*), which combines the kinetic energy of MC collisions and collision frequency [70, 77, 78]:

$$TCS = \left(\frac{m_{MC} u_{MC}}{2}\right) \frac{\left(\frac{u_{MC}\varphi^2}{d_{MC}^2}\right)}{\left(\frac{\varphi}{\frac{\pi}{6} d_{MC}^3}\right)} \tag{27}$$

where m_{MC} is the MC mass, φ is the volume fraction of the MCs (or in general the solid phase) and d_{MC} is the MC diameter. The relative velocity of the MCs u_{MC} depends on the eddy size. If $\lambda \leq d_{MC}$, u_{MC} can be described by Kolmogorov's energy dissipation from Eq. (6) and the *TCS* from Eq. (27) can be changed to:

$$TCS_\lambda = (\varepsilon\nu)^{0.75} \left(\frac{\pi^2 \rho_{MC} d_{MC}^2 \varphi}{72}\right) \tag{28}$$

Larger eddies transport the MCs along their streamlines and the density of these streamlines is a crucial determinant of the frequency of MC collisions, as well as the transport of MCs from one streamline to another and the resulting velocity fluctuation [69, 70]. The MC velocity u_{MC} for larger eddies ($\Lambda > d_{MC}$) depends on the shear rate or velocity gradient:

$$TCS_\Lambda = \left(\frac{\varepsilon}{\nu}\right)^{2/3} \left(\frac{\pi^2 \rho_{MC} d_{MC}^5 \varphi}{72}\right) \tag{29}$$

It is not possible to separate the damaging effect of shear stress and MC collisions, so we recommend a preliminary analysis of shear stress according to Kolmogorov's theory and an assessment of the *TCS* according to the Cherry model (Fig. 2) for the design of MC-based processes [69, 77, 78]. This can be used to determine the working range for the MCs in terms of mixing times [70].

The lower range of our MC stress assessment is the critical agitation rate, which is just sufficient to suspend the MCs. The stirrer speed should be increased until all MCs are suspended, and the critical threshold for complete suspension is reached when no MCs remain longer than 1–2 s on the bioreactor floor. A further increase in the agitation rate leads to a homogenous MC suspension. The critical agitation rate N_c was estimated by Zwietering and colleagues as follows [79]:

$$N_c = S\nu^{0.1} \left(\frac{g(\rho_{MC} - \rho_L)}{\rho_L}\right)^{0.45} X_{MC}^{0.13} d_{MC}^{0.2} d_S^{-0.85} \tag{30}$$

where X_{MC} is the MC concentration and the constant S depends on the stirrer type and d_S/D_T ratio (e.g., $S = 7.7$ for a turbine impeller for which $d_S/D_T = 0.3$ [59]). The Zwietering correlation was developed for high-density particles such as sand and glass [80] and may overestimate N_c for MCs due to the similar density of MCs and the culture medium [81]. However, we found that it closely matched
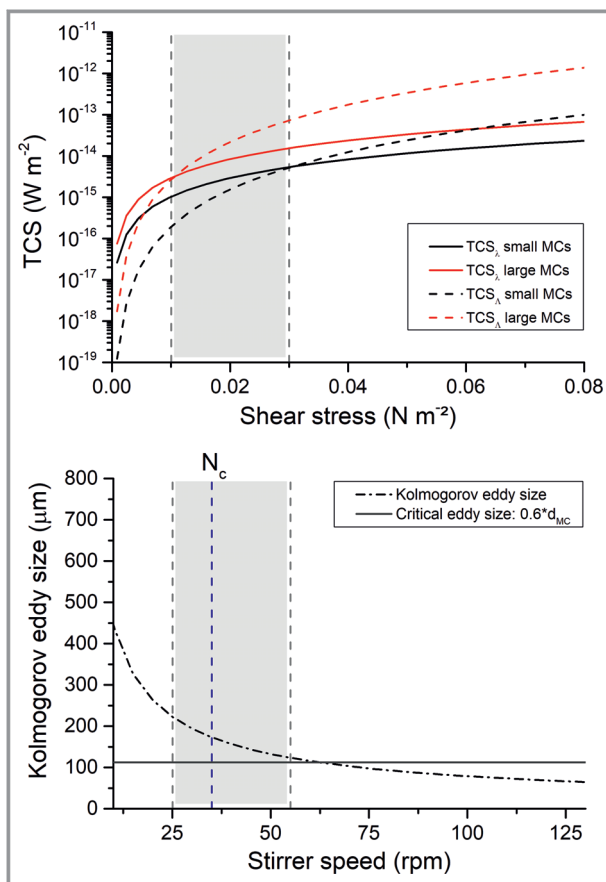
Figure 2. Assessment of the working range (gray area in both diagrams) for the microcarrier-based expansion of hMSCs in a stirred-tank bioreactor (STR) equipped with a Rushton turbine. First, we estimated the turbulent collision severity (*TCS*) for the Kolmogorov range TCS_λ ($\lambda \leq d_{MC}$) and macroscale TCS_Λ ($\Lambda > d_{MC}$) for the smallest and largest MC size distributions. The four resulting curves were correlated against shear stress. At the intersections of TCS_λ (— solid black line) and TCS_Λ (- - - dashed black line) for small MCs at 0.03 N m^{-2} (55 rpm) and TCS_λ (— solid red line) and TCS_Λ (- - - dashed red line) for large MCs at 0.01 N m^{-2} (25 rpm), the macroscale is dominant and provides enough energy for complete suspension of the MCs [53]. These intersections define the lower and upper points of the working range. Second, we calculated the critical agitation speed N_c using the Zwietering correlation [60] (- - - vertical dashed blue line) at 35 rpm and the critical eddy size (- - - horizontal dashed gray line at 112 μm) to prevent cell damage ($\lambda \geq \sim 0.6 d_{MC}$) for the mean MC size (168 μm). The N_c criterion fits well within the defined working range, whereas the intersection of the critical eddy size with the Kolmogorov eddy size (- · - dot-dashed black line) at ~60 rpm confirms the upper limit of the working range.

our empirical data for MCs in real cell culture environments. Loubière et al. [80] applied dimensional analysis and a computational fluid dynamic (CFD) model to different stirrer types and arrangements, as well as the MC concentration, to improve on the Zwietering correlation, confirming the importance of appropriate stirrer selection. Collignon et al. [82] found that the TTP Mixel (axial pumping) and elephant-ear impeller (axial/radial pumping) were

superior for the mixing of MCs under low shear stress conditions and suggested that the spatial liquid velocities for all tested impellers were similar at N_c for MC suspensions. Nevertheless, axial stirrers remain the most popular stirrer type due to their scalability and favorable mixing time, hydrodynamic forces, and oxygen to liquid mass transfer [83]. However, the reported low hydrodynamic stress of axial impellers may be misleading, and the system-dependent hydrodynamics require empirical verification.

Jossen et al. [6] investigated the optimal agitation speed for hMSCs in spinner flasks by applying the N_c criterion. They also compared the influence of heterogeneity at N_c and full suspension. Cell growth was inhibited by an insufficient agitation rate of 25 rpm leading to incomplete MC suspension ($\mu_{max} = 0.026$ h^{-1}, local shear stress = $3.2 \cdot 10^{-3}$ N m^{-2}) and also by a high stirrer speed of 120 rpm ($\mu_{max} = 0.017$ h^{-1}, local shear stress = $13.6 \cdot 10^{-3}$ N m^{-2}, increased lactate production). Optimal cell growth and metabolism was achieved at N_c (49 rpm), which promoted rapid cell growth ($\mu_{max} = 0.029$ h^{-1}, local shear stress = $5 \cdot 10^{-3}$ N m^{-2}). Complete MC suspension was achieved at 63 rpm and marginally reduced cell growth ($\mu_{max} = 0.028$ h^{-1}, local shear stress = $6.7 \cdot 10^{-3}$ N m^{-2}). The inhibition of cell growth at low stirrer speeds reflects the lack of mass transfer, whereas the similar effect at high stirrer speeds reflects the damage caused by excess shear. The upper limit for hydrodynamic forces should not be based solely on cell damaging effects because even lower hydrodynamic forces can prevent successful attachment ($F_{ad} <$ counteracting hydrodynamic forces) or induce unwanted hMSC differentiation [84].

The N_c criterion stands out as the minimal required power input for proper mixing characteristics combined with the lowest possible shear stress, potentially offering a suitable alternative to the typical scale-up criteria based on homogenous energy dissipation (Sect. 3.3). Interestingly, MC agglomeration during cultivation was not significantly more prevalent at N_c (Sauter diameter = 0.58 ± 0.07 mm) than the maximum stirrer speed of 120 rpm (Sauter diameter = 0.55 ± 0.06 mm). This shows that the impaired cell growth at 120 rpm is caused by hydrodynamic stress alone and not by limited mass transfer within the MC agglomerates, because these have a similar size at N_c. This showcases the benefits of optimal STR design in terms of baffles, stirrer type and geometry, rather than solely increasing the stirrer speed during cultivation and accepting the higher shear stress.

A systematic overview of hMSC expansion on MCs in an STR environment is challenging because many publications omit important parameters such as the precise STR geometry, working volume (H_L/D_T), stirrer type, speed, N_P, d_S/D_T, h_S/d_S, baffled vs non-baffled, and culture medium density/viscosity. In many cases, this is because the authors were approaching the study from a biological rather than an engineering perspective. We have summarized the historical data available in the literature (Tab. 2) and in some cases we

Table 2. Summary of STR-based processes for the expansion of hMSCs from different sources. Due to the absence of some key information, we assumed certain parameters such as flow regime (Re, turbulent, transitional) with regard to the installed baffling, geometric arrangement (assumption of dished bottom), final cell density (X_{cell}), cells per microcarrier ($X_{cells/MC}$) and cell-based fold expansion (F_{Ex}). We calculated the prevalent mean (τ_{mean}) and maximum (τ_{max}) shear stress and $\varepsilon_{max}/\bar{\varepsilon}$ ratio according to Eq. (21). PCL = Poly(ε-caprolactone).

hMSC type	STR; $V_{Working}$ [L]; D_T [m]	Stirrer type; d_S [m]; pumping direction; power number N_P [-]	Geometric arrangement D_S/D_T	H_L/D_T	Baffling or probes as baffles	Re range [-] and flow range	Shear stress [N m^{-2}] τ_{mean}	τ_{max}	$\varepsilon_{max}/\varepsilon$ [-]	Microcarrier type and coating	Max. cell density X_{cell} [cells mL^{-1}]	$X_{cells/MC}$ [cells MC^{-1}]	F_{Ex} [-]	Ref.
Bone marrow-derived hMSCs	5 L Biostat B Plus; $V_{Working}$ = 2.5; D_T = 0.16	3-SPB (45°); d_S = 0.07; axial/radial; N_P = 1.2	0.4	2	4 baffles; 3 probes (complete baffling)	8890; transitional to turbulent flow	0.3	0.13	17	Plastic P-102L	1.7·10^5	35	7	[72]
	Mobius 3 L; $V_{Working}$ = 2.4; D_T = 0.14	Marine impeller; d_S = 0.08; axial up-pumping; N_P = 0.3	0.6	1.6	No baffles; 3 probes	6986; transitional flow	0.02	0.06	7	Collagen-coated	0.4·10^5	5	3	[67]
	Mobius 50 L; $V_{Working}$ = 20; D_T = 0.34	4-pitched blade stirrer (13°); d_S = 0.11; axial up-pumping; N_P = 3.2	0.3	1.3	1 baffle	18 393; transitional flow due to low baffling	0.06	0.4	50	Collagen-coated	1.9·10^5	25	13	[69]
Adipose tissue derived hMSCs	MiniBio500; $V_{Working}$ = 0.15; D_T = 0.07	Marine impeller; d_S = 0.03; axial; N_P = 0.4	0.4	1.1	3 probes	1612; transitional flow	0.01	0.03	11	SoloHill® Plastic, coated with α-MEM + 10% FCS	2.7·10^5	36	3	[71]
	UniVessel® SU 2; $V_{Working}$ = 2; D_T = 0.13	2 x 3-SPB (30°); d_S = 0.06; axial/radial; N_P = 1.2	0.4	2.5	No baffles	10 244; transitional flow due to non-baffling	0.05	0.3	26	ProNectin F	2.7·10^5	81	54	[73]
	Cultibag 50L STR; $V_{Working}$ = 35; D_T = 0.37	Combination of Rushton turbine and 3-SPB; d_S = 0.14; axial/radial; N_P = 3.1	0.4	5.2	No baffles	27 206; transitional flow due to non-baffling	0.05	0.4	38	ProNectin F	2.7·10^5	81	54	[73]
Umbilical cord hMSCs	1L BiostatB-DBU; $V_{Working}$ = 0.15; D_T = 0.11	3-SPB (45°); d_S = 0.05; axial/radial; N_P = 1.2	0.4	0.3	3 probes	4459; transitional flow	0.06	0.11	4	porous PCL, coated with fibronectin and poly-L-lysine	4.4·10^5	15	4	[68]
	2.5L Celligen 310; $V_{Working}$ = 0.8; D_T = 0.21	3-SPB (45°); d_S = 0.1; axial/radial; N_P = 1.2	0.5	0.3	3 probes (Tozetti et al.)	7849; intermediate flow	0.04	0.06	2	Cutispher S	1.4·10^5 1.0·10^5	129 45	6 5	[70] [74]

worked with assumptions. Our literature survey produced five important conclusions:

1) most studies used an up-pumping axial stirrer or 45° 3-SPB device, as well as one setup with a combined 3-SPB/Rushton turbine ($N_P = 0.3$–3.1),
2) the d_S/D_T ratio ranged from 0.3–0.5,
3) in most cases, the flow regime was transitional, meaning $Re < 10\,000$ for baffled STRs and $Re < 60\,000$ for non-baffled STRs,
4) the mean energy dissipation was low ($\bar{\varepsilon} = 0.2$–$4.8\,\mathrm{mW\,kg^{-1}}$) resulting in a low mean shear stress of 0.01–0.06 N m^{-2}, and
5) the final hMSC concentration was 0.4–$44 \cdot 10^5\,\mathrm{cells\,mL^{-1}}$ [84–92].

Based on the available data, we found no impact on the scale, hMSC source or MC type. Common parameters in all the STR processes included $d_S/D_T \approx 0.4$, low shear stress and thus a low overall P/V, the installation of axial or axial/radial stirrers, and the establishment of a homogenous MC suspension (upper transitional range) to achieve a sufficient mass transfer. This indicates the robustness and broad working range of MC-based processes for the expansion of hMSCs. The harvest method should receive more attention because the gentle and efficient detachment of cells from the MC is a key step in every MC-based process.
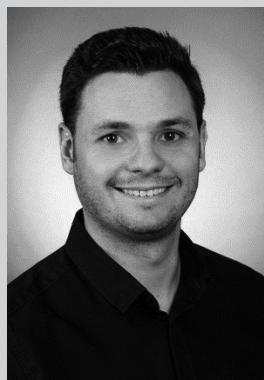
Our recommendations for the MC-based expansion of hMSCs agree with the literature and aim to achieve overall low energy dissipation ($3\,\mathrm{mW\,kg^{-1}}$) while maintaining a low $\varepsilon_{\max}/\bar{\varepsilon}$ ratio (< 20). This can be delivered by the installation of at least four baffles ($B_{I,com}$) and ensuring that $H_L/D_T \approx 1$. The application of N_c guarantees this minimal energy input but limits the potential for hydrodynamic characterization because a turbulent flow regime may not be possible. However, the successful cultivation of hMSCs on various MCs shows that the establishment of a turbulent flow regime is not necessary if a homogenous MC suspension is achieved and sufficient mass transfer is guaranteed. This behavior is favored by the installation of axial stirrers, which are well known for their efficient homogenization and rapid mixing. The higher particle stress may not be relevant due to the low stirrer speeds and resulting low energy dissipation. The combined properties of axial and radial pumping stirrers (45°, 3-SPB) may circumvent the higher particle stress caused by axial stirrers while ensuring sufficient mixing. The installation of a radial stirrer (such as a Rushton turbine) alone is not recommended (low V_S/V_L) but may be beneficial in combination with an axial stirrer. In conclusion, a STR setup with axial and axial/radial stirrers and the following parameters is proposed: $d_S/D_T \geq 0.4$, a high h_S/d_S ratio leading to a high V_S/V_L ratio, and $C \approx 0.2$. This is in agreement with a stirrer design and arrangement optimized using a CFD model for the MC-based expansion of hMSCs, which comprised an elephant-ear impeller with a blade angle of 57°, $d_S/D_T = 0.4$, $C/D_T = 0.5$ and $\varepsilon_{\max} = 0.01\,\mathrm{W\,kg^{-1}}$ [93].

5 Conclusion

A detailed understanding of the hMSC production process is necessary for success, based on both theoretical considerations and empirical testing. Size is a CQA for hMSC spheroids, and although it is not possible to produce spheroids of a uniform size, the process conditions can be adapted to achieve a narrow size distribution with the peak at the desired size. We know that Kolmogorov's theory of isotropic fluctuation can describe the forces acting on cells in a STR but only in a rudimentary manner. Even so, Kolmogorov's theory can be used as a starting point for the production of defined spheroids. It may be possible to correlate the mean energy dissipation $\bar{\varepsilon}$ with the adhesion force F_{ad} between cells. A bioreactor setup that achieves the most homogenous energy dissipation (in practical terms, a low $\varepsilon_{\max}/\bar{\varepsilon}$ ratio) would then be able to produce spheroids with a narrow defined size distribution. A low $\varepsilon_{\max}/\bar{\varepsilon}$ ratio can be achieved by selecting an appropriate stirrer with a high swept volume V_S. We recommend a d_S/D_T ratio ≥ 0.4, a high h_S/d_S ratio (thus a high V_S/V_L ratio) and a bottom clearance of $C \approx 0.2$. A fully turbulent flow regime is also beneficial for this process, which requires complete baffling.

A different STR setup is required for MC-based hMSC production. A full turbulent flow regime is unnecessary if a homogenous MC suspension can be achieved. Even so, we recommend complete suspension to minimize the required power input and enhance the mixing performance. MC suspension can be achieved with the minimum power input/stirrer speed to ensure the MCs are just suspended, but TCS and mixing time investigations also provide valid data for the minimum power input. This is also influenced by the bioreactor and stirrer geometry. The maximum power input is given by the shear stress on the MCs and cells, which can be estimated by correlations such as Kolmogorov's theory and TCS, but we recommend the proper correlation of the upper power limit and hMSC functionality. Further a low energy distribution and a low $\varepsilon_{\max}/\bar{\varepsilon}$ ratio are recommended, both of which are also beneficial for MC-based hMSC production processes.

Florian Petry studied biotechnology and biopharmaceutical technology at the University of Applied Science Mittelhessen (THM), Giessen, Germany. During his Bachelor's degree and internship at Kansas State University in Manhattan, Kansas, USA, and during his Master's degree, he gained experience in the bioreactor-based expansion of animal cells. He is currently a doctoral student at the Institute of Bioprocess Engineering and Pharmaceutical Technology (IBPT) and investigates the agglomeration of insulin-producing β-cells and human mesenchymal stem cells under dynamic conditions, aiming to generate spheroids with a defined size.

Denise Salzig studied biochemistry and was awarded a PhD in bioprocess technology. She currently works at the University of Applied Sciences Mittelhessen (THM) Institute of Bioprocess Engineering and Pharmaceutical Technology (IBPT), Giessen, Germany. In the group of Prof. Dr.-Ing Peter Czermak, she leads the cell culture technology section, which focuses on bioprocesses involving animal cells. Dr.-Ing. Salzig has more than 10 years of experience in stem cell process development, a major focus of her research. Her work includes the implementation of online methods for cultivation control, the development of reactor concepts, and process strategies for diverse applications.

Symbols used

B_I	[–]	baffle index
$B_{I,com}$	[–]	complete baffle index
C	[–]	bottom clearance
C_{Agg}	[–]	aggregate strength coefficient
c_F	[–]	correction factor
D_T	[m]	tank diameter
$d_{P,max}$	[m]	particle size
d_S	[m]	stirrer diameter
d_{MC}	[m]	microcarrier size
d_{Oil}	[m]	oil drop diameter
E_{Kin}	[J]	kinetic energy of fluid
E_{Bond}	[J]	potential energy of spheroid
F_{ad}	[N]	adhesion force
F_{Ex}	[–]	cell-based fold expansion
H_B	[m]	baffle height in liquid
h_S	[m]	height of stirrer
$h_{S,B}$	[m]	height of stirrer from bottom
H_L	[m]	liquid height
k_{cell}	[–]	cell specific dissociation constant
m	[kg]	mass of fluid
m_{MC}	[kg]	mass of microcarrier
N_c	[s^{-1}]	critical suspension speed
n	[s^{-1}]	stirrer frequency
N_B	[–]	number of baffles
N_P	[–]	power number
$N_{P,com}$	[–]	power number for complete baffling
P	[kg m^{2}s^{-3}]	power input
Re	[–]	Reynolds number
S	[–]	bioreactor specific constant
TCS	[–]	turbulent collision severity
t_c	[s]	circulation time
t_M	[s]	mixing time
u	[m s^{-1}]	turbulent fluctuation velocity
u_{MC}	[m s^{-1}]	relative microcarrier velocity
V_L	[m^3]	volume of the fluid
V_S	[m^3]	stirrer swept volume
W_B	[m]	baffle width
X_{cell}	[cells mL^{-1}]	cell concentration
X_{MC}	[g L^{-1}]	microcarrier concentration
$X_{cells/MC}$	[cells MC^{-1}]	cells per microcarrier

Greek symbols

$\dot{\gamma}$	[s^{-1}]	shear rate
ε	[W m^{-3}]	specific energy dissipation
$\bar{\varepsilon}$	[W m^{-3}]	mean energy dissipation
ε_{loc}	[W m^{-3}]	local energy dissipation
ε_{low}	[W m^{-3}]	lowest energy dissipation
ε_{max}	[W m^{-3}]	maximum energy dissipation
η	[kg m^{-1}s^{-1}]	dynamic viscosity
Λ_0	[m]	largest existing eddies
λ	[m]	smallest existing eddies
σ_T	[N m^{-2}]	hydrodynamic tensile stress
σ_S	[N m^{-2}]	hydrodynamic shear stress
τ_L	[N m^{-2}]	laminar shear stress
τ_T	[N m^{-2}]	turbulent shear stress
δ_{Sph}	[N m^{-1}]	pseudo-surface tension of spheroid
μ_{max}	[h^{-1}]	maximum growth rate
ν_L	[m^{2}s^{-1}]	kinematic viscosity
ρ_L	[kg m^{-3}]	fluid density
ρ_{MC}	[kg m^{-3}]	microcarrier density
φ	[–]	volume fraction of the microcarrier/solid phase

Abbreviations

3-SPB	three-segment pitched-blade stirrer
CFD	computational fluid dynamic
CHO	Chinese hamster ovary
CT	cell therapy
CQA	critical quality attribute
ECM	extracellular matrix
EDCF	energy dissipation circulation function
EMA	European Medicines Agency
FDA	Food and Drug Administration
hMSCs	human mesenchymal stromal/stem cells
MC	microcarrier
PS	polystyrene
STR	stirred-tank reactor
VEGF	vascular endothelial growth factor

References

[1] V. Shukla, E. Seoane-Vazquez, S. Fawaz, L. Brown, R. Rodriguez-Monguio, *Hum. Gene Ther.: Clin. Dev.* **2019**, *30 (3)*, 102–113. DOI: https://doi.org/10.1089/humc.2018.201

[2] M. Kabat, I. Bobkov, S. Kumar, M. Grumet, *Stem Cells Transl. Med.* **2020**, *9 (1)*, 17–27. DOI: https://doi.org/10.1002/sctm.19-0202

[3] P. Bajgain, R. Mucharla, J. Wilson, D. Welch, U. Anurathapan, B. Liang, X. Lu, K. Ripple, J. M. Centanni, C. Hall, D. Hsu, L. A. Couture, S. Gupta, A. P. Gee, H. E. Heslop, A. M. Leen, C. M. Rooney, J. F. Vera, *Mol. Ther. – Methods Clin. Dev.* **2014**, *1*, 14015. DOI: https://doi.org/10.1038/mtm.2014.15

[4] C. Weber, D. Freimark, R. Pörtner, P. Pino-Grace, S. Pohl, C. Wallrapp, P. Geigle, P. Czermak, *Int. J. Artif. Organs* **2010**, *33 (11)*, 782–795.

[5] C. Barckhausen, B. Rice, S. Baila, L. Sensebé, H. Schrezenmeier, P. Nold, H. Hackstein, M. T. Rojewski, *Methods Mol. Biol. (Clifton, N.J.)* **2016**, *1416*, 389–412. DOI: https://doi.org/10.1007/978-1-4939-3584-0_23

[6] V. Jossen, C. Schirmer, D. Mostafa Sindi, R. Eibl, M. Kraume, R. Pörtner, D. Eibl, *Stem Cells Int.* **2016**, *2016*, 4760414. DOI: https://doi.org/10.1155/2016/4760414

[7] D. S. Pinto, T. Ahsan, J. Serra, A. Fernandes-Platzgummer, J. M. S. Cabral, C. L. da Silva, *J. Cell. Physiol.* **2020**, *235 (10)*, 7224–7238. DOI: https://doi.org/10.1002/jcp.29622

[8] D. de Sousa Pinto, C. Bandeiras, M. de Almeida Fuzeta, C. A. V. Rodrigues, S. Jung, Y. Hashimura, R.-J. Tseng, W. Milligan, B. Lee, F. C. Ferreira, C. Lobato da Silva, J. M. S. Cabral, *Biotechnol. J.* **2019**, *14 (8)*, e1800716. DOI: https://doi.org/10.1002/biot.201800716

[9] V. Jossen, R. Pörtner, S. C. Kaiser, M. Kraume, D. Eibl, R. Eibl, in *Cells and Biomaterials in Regenerative Medicine* (Ed: D. Eberli), InTech **2014**.

[10] D. Grimm, M. Egli, M. Krüger, S. Riwaldt, T. J. Corydon, S. Kopp, M. Wehland, P. Wise, M. Infanger, V. Mann, A. Sundaresan, *Stem Cells Dev.* **2018**, *27 (12)*, 787–804. DOI: https://doi.org/10.1089/scd.2017.0242

[11] J. Barekzai, F. Petry, J. Zitzmann, P. Czermak, D. Salzig, in *New Advances on Fermentation Processes* (Ed: R. María Martínez-Espinosa), IntechOpen **2020**.

[12] M. N. F. B. Hassan, M. D. Yazid, M. H. M. Yunus, S. R. Chowdhury, Y. Lokanathan, R. B. H. Idrus, A. M. H. Ng, J. X. Law, *Stem Cells Int.* **2020**, *2020*, 9529465. DOI: https://doi.org/10.1155/2020/9529465

[13] H. J. Henzler, Particle Stress in Bioreactors, in *Influence of Stress on Cell Growth and Product Formation* (Eds: K. Schügerl et al.), Advances in Biochemical Engineering/Biotechnology, vol 67, Springer, Berlin **2000**, 35–82. DOI: https://doi.org/10.1007/3-540-47865-5_2

[14] M. Kraume, *Mischen und Rühren: Grundlagen und moderne Verfahren*, Wiley-VCH, Weinheim **2003**.

[15] F. Garcia-Ochoa, V. E. Santos, E. Gomez, Stirred Tank Bioreactors, in *Comprehensive Biotechnology*, Vol. 47, Elsevier, Amsterdam **2011**.

[16] G. Langer, A. Deppe, *Chem. Ing. Tech.* **2000**, *72 (1–2)*, 31–41. DOI: https://doi.org/10.1002/1522-2640(200001)72:1/2<31:aid-cite31>3.0.co;2-o

[17] Y. Petrenko, E. Syková, Š. Kubinová, *Stem Cell Res. Ther.* **2017**, *8 (1)*, 94. DOI: https://doi.org/10.1186/s13287-017-0558-6

[18] Z. Cesarz, K. Tamama, *Stem Cells Int.* **2016**, *2016*, 9176357. DOI: https://doi.org/10.1155/2016/9176357

[19] N.-C. Cheng, S.-Y. Chen, J.-R. Li, T.-H. Young, *Stem Cells Transl. Med.* **2013**, *2 (8)*, 584–594. DOI: https://doi.org/10.5966/sctm.2013-0007

[20] K. C. Murphy, S. Y. Fang, J. K. Leach, *Cell Tissue Res.* **2014**, *357 (1)*, 91–99. DOI: https://doi.org/10.1007/s00441-014-1830-z

[21] S. Sart, A.-C. Tsai, Y. Li, T. Ma, *Tissue Eng., Part B* **2014**, *20 (5)*, 365–380. DOI: https://doi.org/10.1089/ten.TEB.2013.0537

[22] R.-Z. Lin, R.-Z. Lin, H.-Y. Chang, *Biotechnol. J.* **2008**, *3 (9-10)*, 1172–1184. DOI: https://doi.org/10.1002/biot.200700228

[23] J. Hoarau-Véchot, A. Rafii, C. Touboul, J. Pasquier, *Int. J. Mol. Sci.* **2018**, *19 (1)*, 181. DOI: https://doi.org/10.3390/ijms19010181

[24] P. R. Baraniak, M. T. Cooke, R. Saeed, M. A. Kinney, K. M. Fridley, T. C. McDevitt, *J. Mech. Behav. Biomed. Mater.* **2012**, *11*, 63–71. DOI: https://doi.org/10.1016/j.jmbbm.2012.02.018

[25] T. J. Bartosh, J. H. Ylöstalo, A. Mohammadipoor, N. Bazhanov, K. Coble, K. Claypool, R. H. Lee, H. Choi, D. J. Prockop, *Proc. Natl. Acad. Sci. U. S. A.* **2010**, *107 (31)*, 13724–13729. DOI: https://doi.org/10.1073/pnas.1008117107

[26] A.-C. Tsai, Y. Liu, X. Yuan, T. Ma, *Tissue Eng., Part A* **2015**, *21 (9–10)*, 1705–1719. DOI: https://doi.org/10.1089/ten.TEA.2014.0314

[27] M. Deynoux, N. Sunter, E. Ducrocq, H. Dakik, R. Guibon, J. Burlaud-Gaillard, L. Brisson, F. Rouleux-Bonnin, L.-R. Le Nail, O. Hérault, J. Domenech, P. Roingeard, G. Fromont, F. Mazurier, *PLoS one* **2020**, *15 (6)*, e0225485. DOI: https://doi.org/10.1371/journal.pone.0225485

[28] J. H. Lee, Y.-S. Han, S. H. Lee, *Biomol. Ther.* **2016**, *24 (3)*, 260–267. DOI: https://doi.org/10.4062/biomolther.2015.146

[29] X. Cui, Y. Hartanto, H. Zhang, *J. R. Soc., Interface* **2017**, *14 (127)*. DOI: https://doi.org/10.1098/rsif.2016.0877

[30] M. A. Kinney, C. Y. Sargent, T. C. McDevitt, *Tissue Eng., Part B* **2011**, *17 (4)*, 249–262. DOI: https://doi.org/10.1089/ten.teb.2011.0040

[31] A. Sen, M. S. Kallos, L. A. Behie, *Ind. Eng. Chem. Res.* **2001**, *40 (23)*, 5350–5357. DOI: https://doi.org/10.1021/ie001107y

[32] J. Rouwkema, B. F. J. M. Koopman, C. A. van Blitterswijk, W. J. A. Dhert, J. Malda, *Biotechnol. Genet. Eng. Rev.* **2009**, *26 (1)*, 163–178. DOI: https://doi.org/10.5661/bger-26-163

[33] K. C. Murphy, B. P. Hung, S. Browne-Bourne, D. Zhou, J. Yeung, D. C. Genetos, J. K. Leach, *J. R. Soc., Interface* **2017**, *14 (127)*. DOI: https://doi.org/10.1098/rsif.2016.0851

[34] D. R. Grimes, C. Kelly, K. Bloch, M. Partridge, *J. R. Soc., Interface* **2014**, *11 (92)*, 20131124. DOI: https://doi.org/10.1098/rsif.2013.1124

[35] H.-J. Henzler, *Chem. Ing. Tech.* **1982**, *54 (5)*, 461–476. DOI: https://doi.org/10.1002/cite.330540510

[36] F. Petry, T. Weidner, P. Czermak, D. Salzig, *Stem Cells Int.* **2018**, *2018*, 2547098. DOI: https://doi.org/10.1155/2018/2547098

[37] B. Maiorella, G. Dorin, A. Carion, D. Harano, *Biotechnol. Bioeng.* **1991**, *37 (2)*, 121–126. DOI: https://doi.org/10.1002/bit.260370205

[38] T. A. Wyrobnik, A. Ducci, M. Micheletti, *Stem Cell Res.* **2020**, *47*, 101888. DOI: https://doi.org/10.1016/j.scr.2020.101888

[39] D. J. Karst, E. Serra, T. K. Villiger, M. Soos, M. Morbidelli, *Biochem. Eng. J.* **2016**, *110*, 17–26. DOI: https://doi.org/10.1016/j.bej.2016.02.003

[40] J. Zitzmann, *Prozessintensivierung für die Produktion von antimikrobiellen Peptiden mit stabil transfizierten Drosophila melanogaster S2-Zelllinien*, Schriftenreihe des Institutes für Bioverfahrenstechnik und Pharmazeutische Technologie, Band 14, Shaker Verlag, Düren **2019**.

[41] C. J. Hewitt, K. Lee, A. W. Nienow, R. J. Thomas, M. Smith, C. R. Thomas, *Biotechnol. Lett.* **2011**, *33 (11)*, 2325–2335. DOI: https://doi.org/10.1007/s10529-011-0695-4

[42] G. Pattappa, H. K. Heywood, J. D. de Bruijn, D. A. Lee, *J. Cell. Physiol.* **2011**, *226 (10)*, 2562–2570. DOI: https://doi.org/10.1002/jcp.22605

[43] S. Wollny, *Experimentelle und numerische Untersuchungen zur Partikelbeanspruchung in gerührten (Bio-)Reaktoren*, Dissertation, Technische Universität Berlin **2010**.

[44] K. Mühle, K. Domasch, *Chem. Eng. Process.* **1991**, *29 (1)*, 1–8. DOI: https://doi.org/10.1016/0255-2701(91)87001-J

[45] R. Wengeler, H. Nirschl, *J. Colloid Interface Sci.* **2007**, *306 (2)*, 262–273. DOI: https://doi.org/10.1016/j.jcis.2006.10.065

[46] H. Schubert, K. Mühle, *Adv. Powder Technol.* **1991**, *2 (4)*, 295–306. DOI: https://doi.org/10.1016/S0921-8831(08)60696-2

[47] P. Jarvis, B. Jefferson, J. Gregory, S. A. Parsons, *Water Res.* **2005**, *39 (14)*, 3121–3137. DOI: https://doi.org/10.1016/j.watres.2005.05.022

[48] B. Oyegbile, P. Ay, S. Narra, *Environ. Eng. Res.* **2016**, *21 (1)*, 1–14. DOI: https://doi.org/10.4491/eer.2015.086

[49] M. Kobayashi, Y. Adachi, S. Ooi, *Proc. Hydraul. Eng.* **2001**, *45*, 1249–1253. DOI: https://doi.org/10.2208/prohe.45.1249

[50] P. Jüsten, G. C. Paul, A. W. Nienow, C. R. Thomas, *Biotechnol. Bioeng.* **1996**, *52 (6)*, 672–684. DOI: https://doi.org/10.1002/(SICI)1097-0290(19961220)52:6<672:AID-BIT5>3.0.CO;2-L

[51] L. Böhm, L. Hohl, C. Bliatsiou, M. Kraume, *Chem. Ing. Tech.* **2019**, *91 (12)*, 1724–1746. DOI: https://doi.org/10.1002/cite.201900165

[52] R. Vieweg, *Z. Chem.* **1988**, *28 (11)*, 417–418. DOI: https://doi.org/10.1002/zfch.19880281120

[53] T. T. Goodman, J. Chen, K. Matveev, S. H. Pun, *Biotechnol. Bioeng.* **2008**, *101 (2)*, 388–399. DOI: https://doi.org/10.1002/bit.21910

[54] A. Yeung, A. Gibbs, R. Pelton, *J. Colloid Interface Sci.* **1997**, *196 (1)*, 113–115. DOI: https://doi.org/10.1006/jcis.1997.5140

[55] J. Moreira, P. E. Cruz, P. C. Santana, J. G. Aunins, M. J. T. Carrondo, *Chem. Eng. Sci.* **1995**, *50 (17)*, 2747–2764. DOI: https://doi.org/10.1016/0009-2509(95)00118-O

[56] B. David, in *Principles of cellular engineering: Understanding the biomolecular interface* (Ed: M. R. King), Elsevier Academic Press, Amsterdam **2006**.

[57] C. Löffelholz, S. C. Kaiser, M. Kraume, R. Eibl, D. Eibl, in *Disposable Bioreactors II* (Eds: D. Eibl, R. Eibl), Advances in Biochemical Engineering/Biotechnology, vol 138, Springer, Berlin **2014**, 1–44. DOI: https://doi.org/10.1007/10_2013_187

[58] J. M. Vlak, *Insect cell cultures: Fundamental and applied aspects*, Current applications in cell culture engineering, vol. 2, Kluwer, Dordrecht **1996**.

[59] P. M. Doran, *Bioprocess engineering principles*, 2nd ed., Academic Press, Waltham, MA **2013**.

[60] A. Heyter, S. Wollny, *Chem. Ing. Tech.* **2017**, *89 (4)*, 416–423. DOI: https://doi.org/10.1002/cite.201600188

[61] *Rührwerke: Theoretische Grundlagen, Auslegung und Bewertung* (Eds: F. Liepe, R. Sperling, S. Jembere), 1st ed., Fachhochschule Anhalt, Köthen **1998**.

[62] M. Kraume, *Transportvorgänge in der Verfahrenstechnik: Grundlagen und apparative Umsetzungen*, 2nd ed., VDI Verfahrenstechnik, Springer Vieweg, Berlin **2012**.

[63] M. Zlokarnik, *Stirring: Theory and practice*, Wiley-VCH, Weinheim **2010**.

[64] C. P. Peter, *Auslegung geschüttelter Bioreaktoren für hochviskose und hydromechanisch empfindliche Fermentationssysteme = Design of shaken bioreactors for fermentation systems with elevated viscosity and hydromechanical sensibility*, Dissertation, RWTH Aachen **2007**.

[65] P. S. Couto, A. Bersenev, Q. A. Rafiq, in *Engineering Strategies for Regenerative Medicine* (Eds: T. G. Fernandes, M. M. Diego, J. M. S. Cabral), Elsevier, Amsterdam **2020**.

[66] A. L. van Wezel, *Nature* **1967**, *216 (5110)*, 64–65. DOI: https://doi.org/10.1038/216064a0

[67] A.-C. Tsai, R. Jeske, X. Chen, X. Yuan, Y. Li, *Front. Bioeng. Biotechnol.* **2020**, *8*, 640. DOI: https://doi.org/10.3389/fbioe.2020.00640

[68] J. Leber, J. Barekzai, M. Blumenstock, B. Pospisil, D. Salzig, P. Czermak, *Process Biochem.* **2017**, *59*, 255–265. DOI: https://doi.org/10.1016/j.procbio.2017.03.017

[69] R. S. Cherry, E. T. Papoutsakis, *Bioprocess Eng.* **1986**, *1 (1)*, 29–41. DOI: https://doi.org/10.1007/BF00369462

[70] T. A. Grein, D. Loewe, H. Dieken, T. Weidner, D. Salzig, P. Czermak, *Front. Bioeng Biotechnol.* **2019**, *7*, 78. DOI: https://doi.org/10.3389/fbioe.2019.00078

[71] C. F. Crouch, H. W. Fowler, R. E. Spier, *J. Chem. Technol. Biotechnol.* **1985**, *35 (4)*, 273–281. DOI: https://doi.org/10.1002/jctb.280350408

[72] *Cell Adhesion in Bioprocessing and Biotechnology* (Eds: M. Hjortso, J. W. Roos), CRC Press, Boca Raton, FL **2017**.

[73] J. D. Berry, P. Liovic, I. D. Šutalo, R. L. Stewart, V. Glattauer, L. Meagher, *Appl. Math. Modell.* **2016**, *40 (15–16)*, 6787–6804. DOI: https://doi.org/10.1016/j.apm.2016.02.025

[74] A. W. Nienow, C. J. Hewitt, T. R. J. Heathman, V. A. M. Glyn, G. N. Fonte, M. P. Hanga, K. Coopman, Q. A. Rafiq, *Biochem. Eng. J.* **2016**, *108*, 24–29. DOI: https://doi.org/10.1016/j.bej.2015.08.003

[75] B. Rentier, E. L. Hooghe-Peters, M. Dubois-Dalcq, *J. Virol.* **1978**, *28 (2)*, 567–577.

[76] M. Ludlow, K. Lemon, R. D. de Vries, S. McQuaid, E. L. Millar, G. van Amerongen, S. Yüksel, R. J. Verburgh, A. D. M. E. Osterhaus, R. L. de Swart, W. P. Duprex, *J. Virol.* **2013**, *87 (7)*, 4033–4042. DOI: https://doi.org/10.1128/JVI.03258-12

[77] R. S. Cherry, E. T. Papoutsakis, *Biotechnol. Bioeng.* **1988**, *32 (8)*, 1001–1014. DOI: https://doi.org/10.1002/bit.260320808

[78] R. S. Cherry, E. T. Papoutsakis, *Bioprocess Eng.* **1989**, *4 (2)*, 81–89. DOI: https://doi.org/10.1007/BF00373735

[79] T. N. Zwietering, *Chem. Eng. Sci.* **1958**, *8 (3–4)*, 244–253. DOI: https://doi.org/10.1016/0009-2509(58)85031-9

[80] C. Loubière, A. Delafosse, E. Guedon, I. Chevalot, D. Toye, E. Olmos, *Chem. Eng. Sci.* **2019**, *203*, 464–474. DOI: https://doi.org/10.1016/j.ces.2019.04.001

[81] S. Ibrahim, A. W. Nienow, *Chem. Eng. Res. Des.* **2004**, *82 (9)*, 1082–1088. DOI: https://doi.org/10.1205/cerd.82.9.1082.44161

[82] M.-L. Collignon, A. Delafosse, M. Crine, D. Toye, *Chem. Eng. Sci.* **2010**, *65 (22)*, 5929–5941. DOI: https://doi.org/10.1016/j.ces.2010.08.027

[83] E. Olmos, K. Loubiere, C. Martin, G. Delaplace, A. Marc, *Chem. Eng. Sci.* **2015**, *122*, 545–554. DOI: https://doi.org/10.1016/j.ces.2014.08.063

[84] T. R. J. Heathman, A. W. Nienow, Q. A. Rafiq, K. Coopman, B. Kara, C. J. Hewitt, *Biochem. Eng. J.* **2018**, *136*, 9–17. DOI: https://doi.org/10.1016/j.bej.2018.04.011

[85] Q. A. Rafiq, K. M. Brosnan, K. Coopman, A. W. Nienow, C. J. Hewitt, *Biotechnol. Lett.* **2013**, *35 (8)*, 1233–1245. DOI: https://doi.org/10.1007/s10529-013-1211-9

[86] K. Cierpka, C. L. Elseberg, K. Niss, M. Kassem, D. Salzig, P. Czermak, *Chem. Ing. Tech.* **2013**, *85 (1–2)*, 67–75. DOI: https://doi.org/10.1002/cite.201200151

[87] T. Lawson, D. E. Kehoe, A. C. Schnitzler, P. J. Rapiejko, K. A. Der, K. Philbrick, S. Punreddy, S. Rigby, R. Smith, Q. Feng, J. R. Murrell, M. S. Rook, *Biochem. Eng. J.* **2017**, *120*, 49–62. DOI: https://doi.org/10.1016/j.bej.2016.11.020

[88] F. Moreira, A. Mizukami, L. E. B. de Souza, J. M. S. Cabral, C. L. da Silva, D. T. Covas, K. Swiech, *Front. Bioeng. Biotechnol.* **2020**, *8*, 307. DOI: https://doi.org/10.3389/fbioe.2020.00307

[89] A. T.-L. Lam, J. Li, J. P.-W. Toh, E. J.-H. Sim, A. K.-L. Chen, J. K.-Y. Chan, M. Choolani, S. Reuveny, W. R. Birch, S. K.-W. Oh, *Cytotherapy* **2017**, *19 (3)*, 419–432. DOI: https://doi.org/10.1016/j.jcyt.2016.11.009

[90] A. Mizukami, M. S. de Abreu Neto, F. Moreira, A. Fernandes-Platzgummer, Y.-F. Huang, W. Milligan, J. M. S. Cabral, C. L. da Silva, D. T. Covas, K. Swiech, *Stem Cell Rev. Rep.* **2018**, *14*, 141–143. DOI: https://doi.org/10.1007/s12015-017-9787-4

[91] P. A. Tozetti, S. R. Caruso, A. Mizukami, T. R. Fernandes, F. B. da Silva, F. Traina, D. T. Covas, M. D. Orellana, K. Swiech, *Biotechnol. Prog.* **2017**, *33 (5)*, 1358–1367. DOI: https://doi.org/10.1002/btpr.2494

[92] C. Schirmaier, V. Jossen, S. C. Kaiser, F. Jüngerkes, S. Brill, A. Safa-vi-Nab, A. Siehoff, C. van den Bos, D. Eibl, R. Eibl, *Eng. Life Sci.* **2014**, *14 (3)*, 292–303. DOI: https://doi.org/10.1002/elsc.201300134

[93] C. Loubière, A. Delafosse, E. Guedon, D. Toye, I. Chevalot, E. Olmos, *Chem. Eng. Technol.* **2019**, *42 (8)*, 1702–1708. DOI: https://doi.org/10.1002/ceat.201900105